The Crystal Structure of Mammalian Inositol 1,3,4,5,6-Pentakisphosphate 2-Kinase Reveals a New Zinc Binding Site and Key Features for Protein Function

Elsa Franco-Echevarría[a], Julia Sanz-Aparicio[a], Charles A. Brearley[b], Juana M[a] González-Rubio[a] and Beatriz González [a#]

a *Departamento de Cristalografía y Biología Estructural, Instituto de Química-Física "Rocasolano," CSIC, Serrano 119, 28006-Madrid, Spain*

b *School of Biological Sciences, University of East Anglia, Norwich Research Park, Norwich NR4 7TJ, United Kingdom*

To whom correspondence should be addressed: B. González. Tel.: (+34)-91-5619400; Fax: (+34)-91-564-24-31; E-mail: xbeatriz@iqfr.csic.es.

Running title: Structure of a mammal IP_5 2-K

Keywords: Inositol phosphate, Zinc, crystal structure, structure-function, enzyme mutation, IP_5 2-Kinase, inositol hexakisphosphate

ABSTRACT

Inositol 1,3,4,5,6-pentakisphosphate 2-kinases (IP_5 2-Ks) comprise a family of enzymes in charge of synthesizing inositol hexakisphosphate (IP_6) in eukaryotic cells. This protein and its product IP_6 present many roles in cells, participating in mRNA export, embryonic development, and apoptosis. We reported previously that the full-length IP_5 2-K from *Arabidopsis thaliana* (*At*) is a zinc metallo-enzyme including two separated lobes (the N and C lobes). We have also shown conformational changes in IP_5 2-K and have identified the residues involved in substrate recognition and catalysis. However, the specific features of mammalian IP_5 2-Ks remain unknown. To this end, we report here the first structure for a murine IP_5 2-K in complex with ATP/IP_5 or IP_6. Our structural findings indicated that the general folding in N and C lobes is conserved with *At*IP5 2-K. A helical scaffold in the C lobe constitutes the inositol phosphate (IP)-binding site, which, along with the participation of the N lobe, endows high specificity to this protein. However, we also noted large structural differences between the orthologous from these two eukaryotic kingdoms. These differences include a novel zinc-binding site and regions unique to the mammalian IP_5 2-K, as an unexpected basic patch on the protein surface. In conclusion, our findings have uncovered distinct features of a mammalian IP_5 2-K and set the stage for investigations into protein-protein or protein-RNA interactions important for IP_5 2-K function and activity.

Inositol 1,3,4,5,6-pentakisphosphate 2-kinase (IP_5 2-K) is a key enzyme of higher inositol phosphate (inositide, IP) metabolism. IP_5 2-K is present from yeast to mammals and catalyzes the synthesis of phytic acid (inositol hexakisphosphate or IP_6) from IP_5 and ATP (1). A variety of roles have been proposed for this enzyme and its product IP_6 (2), in DNA repair (3), mRNA editing, export and degradation (4,5), vesicle trafficking (6) and protein ubiquitylation (7). At a molecular level, IP_6 acts as a cofactor for proteins with DNA-dependent protein kinase activity in non-homologous end joining (8) and with GLE1 in mRNA export (4). IP_6 also can act as a folding factor as in the case of adenosine deaminase that participates in editing of mRNA and tRNA (5). In addition, IP_6 is the precursor of inositol pyrophosphates, essential for cellular energy homeostasis, signal transduction control and apoptosis (9,10). Mice embryos with IP_5 2-K deletion do not survive more than a few weeks

(11). More recently a role in ribosomal rRNA synthesis independent of IP_5 2-K catalytic function has been proposed for the human enzyme (12), which has been shown to co-localize with mRNA either in nucleus or cytoplasm (13). All these findings increase the potential of this enzyme as an attractive target.

IP_5 2-K belongs to the inositol polyphosphate (IPK) structural family that include enzymes capable of phosphorylating hydroxyls at different positions of the inositol ring starting from inositol 1,4,5-trisphosphate (IP_3), a well-known second messenger responsible for calcium mobilization (14). These phosphorylation events occur in combination with another family of inositol kinases that adopts a "ATP-grasp like" fold (15,16). Both families together cover a great range of phosphorylation reactions on the six -OH positions of the *myo*-inositol ring and even on those already phosphorylated (15,17,18). Many of these enzymes present redundant abilities acting on similar substrates or they bind an inositide in different orientations that is thus phosphorylated in different positions (19). In contrast, IP_5 2-K is the unique IPK whose physiological role is the phosphorylation of the axial 2-OH position of *myo* inositol, the other five hydroxyls being in equatorial positions. It is also a very specific enzyme and, together with IP_3 3-K, phosphorylates just one position of inositol (20,21).

IPK enzymes are classified as a structural subgroup of protein kinases (PK) family, since they conserve a few features including a fold in two separated lobes (N- and C-lobe) and similar nucleotide recognition mode (22). In addition, the core of the N-lobe is conserved as well as the presence of a few residues involved in catalysis and in nucleotide phosphates binding. In 2004, the first structure of an IPK was described, that from IP_3 3-K (23). Since then, the structure of at least one member of each IPK subfamily has been reported (23-26). In summary, the IPK family presents a specific and characteristic fold in the C-lobe different from PKs, having a β-sheet core with helical insertions showing a great range of sizes depending on the IPK class. These helical regions are involved in substrate binding and have been named by us as IP-lobe or CIP-lobe (19). Thus, promiscuous IPKs, such as the IP multikinases (IPmKs), have a single helix inserted showing an open active site able to cope with various substrates and products, whereas more specific enzymes as IP_3 3-K and IP_5 2-K show larger helical scaffolds. In fact, IP_5 2-K shows the most elaborated helical region.

The full length structure of IP_5 2-K from *Arabidopsis thaliana* (*At*IP_5 2-K) is the only one known for this subfamily (25). It shows the features described above and that it is a zinc metallo-enzyme, for which a structural role has been proposed (25). We subsequently captured different IP_5 2-K conformations by X-ray Crystallography (27) displaying open, half-closed or closed conformations, as the nucleotide and/or the inositide are absent or present in the active site. Extensive work by others and us has identified the residues involved in substrate recognition and catalysis and has depicted the participation of the N-lobe in achievement of a productive conformation (25,27-30). The structure of *At*IP_5 2-K was an important advance for this field but, nevertheless, the specific features of mammal IP_5 2-K remain unknown. IP_5 2-K family shows moderate sequence conservation across the species. In particular, mammalian enzymes show different insertions and do not conserve the zinc site found in the plant enzyme, making difficult to obtain a good sequence alignment. From its sequence motifs, putative zinc binding residues have been proposed in human IP_5 2-K (13). However, if mammal IP_5 2-K is a Zinc metalloenzyme and the putative role for this metal awaits further studies. Because of the significance of IP_5 2-K to proper cell functioning and the many roles of its product IP_6, it is important to understand the molecular basis that underlies this enzyme function. In this work, we have determined the mouse IP_5 2-K structure in presence of inositide showing that, although this enzyme conserves features with the plant enzyme, it differs significantly in many aspects. Our results define the specific features of mammal IP_5 2-Ks. In addition, we present here valuable information that could help in understanding IP_5 2-K functions beyond its catalytic activity as its role in ribosomal RNA synthesis (12)

RESULTS

The structure of IP_5 2-K mammalian isoform-We have solved the structure of *Mus musculus* IP_5 2-K (*m*IP_5 2-K) at 2.4 Å resolution

(Table 1) from a truncated form lacking the 21-C-terminal residues (ΔC-*m*IP_5 2-K). Noticeably, *m*IP_5 2-K crystals were not obtained in absence of the inositide. The structure for *m*IP_5 2-K in presence of one or both ligands, forming binary complexes (IP_6) or ternary complexes (IP_5+ATP) is presented (Fig. S1). In addition, we present two different crystal forms, including one or two molecules in the asymmetric unit respectively, the first showing much better resolution (2.4 *vs* 3.2 Å). As mouse and human IP_5 2-K isoforms shares 91% of sequence identity, we propose the structure of the mouse enzyme as a template for the mammalian IP_5 2-Ks.

Mouse IP_5 2-K folds in two lobes, N- and C- terminal lobes, connected by a hinge therefore conserving the general fold scheme of PKs and IPKs and in a similar way, both lobes co-ordinate the nucleotide between them (Fig. 1*A*). The N-lobe core forms a β-sheet formed by five antiparallel β-strands (β1- β5) showing two helical segments. The first helical segment (N-I) harbors α1, equivalent to the helix αC characterized in all protein kinases, while the second one (N-II) is a specific insertion different in every IPK subfamily. A role of this region for substrate binding in the IP_5 2-K subfamily has been previously reported by others (29) and by us (25,27). Regarding the C-lobe, it also presents a β-sheet core formed by five antiparallel β-strands (β6-β10). Three helical segments are inserted in the β-sheet core. These segments altogether form a large helical ensemble named as CIP lobe in the structure of *At*IP_5 2-K (25), and each of them is consequently named as CIP_I, CIP_{II} and CIP_{III}. The CIP lobe represents more than a half of the protein and is specific to IP_5 2-K enzymes. It creates a scaffold that builds up most of the inositide substrate binding site. The five loops (CL1-CL5) joining the CIP region to the C-lobe β-sheet core are essential since they play a key role in substrate binding and catalysis. (Fig. 1*B* and 2).

mIP_5 2-K active site and substrates recognition-A general view of IP_5 2-K substrate recognition is shown in Fig. 2*A* and detailed in Table S1. The adenine is strongly recognized through polar and hydrophobic interactions with both protein lobes and the hinge connecting them (Fig. 2*B*). In particular, it forms polar interactions with His14 and the backbones of Pro116 and Leu118. The ribose OHs interact with the C-lobe residues Glu136 and Arg209. The triphosphate moiety is tightly bound to the N-lobe of the enzyme through polar interactions and to the C-lobe through two magnesium ions. In particular, phosphate interaction with the residue Arg33, with a flexible loop (G-loop, residues Gly15-Ser20) and with an acidic residue (Asp437) through the Mg ions is conserved throughout the PK superfamily and are essential for nucleotide binding and kinase activity.

Regarding the inositide substrate, IP_5 is tightly bound to the enzyme through its five phosphates (Fig. 2*C*). A total of fourteen residues coordinate the phosphate groups, two of them through water molecules and eight of them being lysine or arginine. P1 and P3 are coordinated by both lobes, while P4-P5 are coordinated exclusively by the C-lobe. Residues from the N-lobe involved in P1 and P3 binding come from the segment N-II (Arg100) and the G-loop (Asn18 and Lys19) mentioned above. Residues from the C-lobe involved in coordination of the five phosphates come from the CIP lobe and its CLs. Fig. 2*C* and Table S1 show all the polar interactions produced with the inositide phosphates (P1: Asn18, Arg100, Lys 138, Lys173 and Asn206; P3: Asn18, Lys19 and Lys441; P4: Gln449; P5: with Lys140, Arg 160 and His164 through water molecules and P6: Lys138, Lys140, Lys168, Asn206 and water mediated with Asn207). The tight and extensive recognition explains the high specificity of this enzyme. Human IP_5 2-K displays a 0.43 μM K_m for IP_5 (31) in good agreement to the value obtained for *m*IP_5 2-K by us (0.29 μM) (Fig. 3*A*) and in contrast with the low tens of micromolar value reported for the *At*IP_5 2-K (22 μM) (32). A possible explanation to the different K_m found in the plant enzyme might be related to some differences found in enzymes from both kingdoms either in the inositide recognition mode or in the constraints introduced by the Zinc binding site (see later).

Six residues from the CLs form the interface of substrates recognition, generating a net of interactions including the Mg ions (Fig. 2*D*). Residues Lys138 and Asp400 make direct interaction with Pγ and/or the nucleophile 2-OH. The distance between the 2-OH and Pγ oxygen is 3.2 Å suggesting an in-line transference

mechanism probably in agreement with an associative mechanism. Pγ is oriented through a Mg ion (Mg1) coordinated to Asp437 and to Asp439 in a second sphere. Asp437 also coordinates a second Mg ion (Mg2) together with Ser402 through a water molecule. Comparison of the ternary and binary complexes (IP_5 2-K/IP_5/ATP *vs* IP_5 2-K/IP_6) shows that there is no significant structural variation among them (r.m.s.d is 0.377 Å for 403 Cα atoms). The IP_6 shows similar interactions, with P2 remaining at the substrates interface region described above.

A BLAST search using *m*IP_5 2-K sequence and limited to mammals (taxid:40674) show that all residues coordinating the nucleotide and inositide are absolutely conserved, just a couple of residues showing a conservative change in some species.

Unexpectedly, the formation of the ternary complex (*m*IP_5 2-K + IP_5 + ATP) was achieved by protein incubation with IP_6 and ADP (Fig. S1). Therefore, we checked that our crystallized *m*IP_5 2-K samples are able to catalyze both the forward (Fig. 3*B*) and reverse (Fig. 3*C*) reactions in solution. In agreement, the plant enzyme is highly reversible with an equilibrium constant in the forward 'kinase' direction of approximately 14 (20). By ion-pair reverse phase HPLC, we were also able to confirm the production of ATP from IP_6 and ADP (data not shown).

Mammal IP_5 2-Ks share a zinc binding site with a novel structure-mIP_5 2-K presents two zinc ions in its structure, one in the CIP-lobe (Zn1) and the other close to the hinge region (Zn2) (Fig. 1 and 4). In fact, Zn1 is present in all the crystals obtained whereas Zn2 was only detected in the low resolution ΔC-*m*IP_5 2-K crystals in which the two molecules in the asymmetric unit interact through the hinge region probably fixing a conformation captured by crystallography (Fig. S2).

The Zn1 site is formed by residues from two CIP lobe elements: Cys159, Cys162 and Cys181 from CIP-I and Cys291 from CIP-II (Fig. 4*A*). This site presents the typical zinc geometry and coordination though it has no homologues in the structural databases using DALI server (33). The two first cysteines from CIP-I are located in an helix, separated by two residues and could remind a partial zinc-finger; however the fourth ligand breaks any resemblance since it comes from a position very distant in sequence. In fact, Cys291 comes from a very long loop inserted into two helices that cross over the back of the CIP-lobe (Fig. 5). We have selected Cys181 and Cys291 as candidates for the mutagenic study (Fig. 4*C*). However, there was no expression of C181S *m*IP_5 2-K mutant in the conditions reported herein for the wild-type protein. This suggests that Zn1 site formation could be essential for proper protein folding. By contrast, C291S *m*IP_5 2-K mutant expression levels are in the same order to the wild-type being only 2-fold decreased. In spite of this, the impact of this mutation on enzyme activity is very high, since the mutated sample retains less than 10% of enzyme activity (Fig. 4*C*). In this line, it is worth mentioning that the two first cysteines of this zinc site are in helix α4, an element that provides four residues for the inositide substrate binding (Fig. 2*A*). We also consider that this fact could have some effect in obtaining a lower K_m for the substrate in *m*IP_5 2-K.

Regarding Zn2, it is created by two residues from the hinge (His125 and His129) and one residue from the C-lobe (Cys410) (Fig. 4*B*). Mutation of residues His129 and Cys410 to serine produces samples with a moderate decrease in enzymatic activity revealing that the Zn2 is not critical for protein function (Fig. 4*C*). A possible explanation for the greater decrease found in H129S mutant could its key location in the hinge, an element important for enzyme flexibility.

We have subsequently evaluated the metal content in *m*IP_5 2-K samples by Inductively Coupled Plasma-Optical Emission Spectroscopy (ICP-OES) (Fig. 4*D*). We confirmed that *m*IP_5 2-K is a Zinc metelloenzime (Table S2). Unexpectedly, wild-type samples purified as LSLt-tagged protein exhibit a zinc:protein molar ratio of 0.6:1. An insufficient supply of zinc could also explain the difficulties encountered in the crystallization process of this enzyme due to structural inhomogeneity. However, attempts to add zinc from different salts to the crystallization drops failed since the protein precipitated. We found a zinc:protein molar ratio of 0.8:1, 0.4:1, and 0.7:1 for H129S, C291S, and C410S, mutants respectively. As expected, mutation on residue Cys291 (Zn1 site) yields an enzyme with less content of zinc than the wild type (Fig. 4*D* and Table S2). By contrast, mutation of Zn2

coordinating residues (His129 and Cys410) yield samples with no reduction in the zinc content (Fig. 4*D* and Table S2). Therefore, we further analyzed the features of the C291S mutant by Circular Dichroism (CD) (Fig. 4*E*). We found that both, WT (wild type) and C291S *m*IP_5 2-K samples display a similar Far-UV CD spectra suggesting that they share similar secondary structural elements. However, thermal denaturation followed by CD revealed that the mutated sample exerts an apparent Tm (32 ºC) drastically reduced compared to that of the WT sample (43 ºC).

In conclusion, our results suggest that Zn1 is necessary for protein folding and stability. Furthermore, the reduced capacity of C291S mutant to bind zinc correlates with a high reduction in protein activity (Fig. 4*C* and 4*D*). In agreement, IP_5 2-Ks from mammals show conservation only in the Zn1 site, its four cysteine ligands being fully conserved. Therefore, Zn1 is key in all mammal IP_5 2-K enzymes whereas Zn2 could be an artifact of crystallization.

Mammal and plant IP_5 2-Ks show three large structural divergences-Up to now, the other IP_5 2-K with known structure is that from *A. thaliana* (25). A Cα superposition of *m*IP_5 2-K onto *At*IP_5 2-K (pdb code 2xan) overlays 327 residues (out of 468 in *m*IP_5 2-K) with an r.m.s.d.= 1.2 Å. A good sequence alignment between both enzymes has remained elusive since their sequence homology is not very high (24% identity and 38% similarity) and they present different insertions. A structural alignment of both IP_5 2-K isoforms is shown in Fig. 5. While the topology of N- and C-lobe cores and substrate binding region are quite conserved, both enzymes present multiple dissimilarities.

The most predominant divergences are found within three regions, which show large differences in their sequence, length and topology (Fig. 5 and 6*A*-*D*). The first main difference (D1) is located in N-I region, *At*IP_5 2-K having an insertion not present in the mammal enzyme (Fig. 6*B*). A possible function of this segment will be discussed below. The second clear difference (D2) is concentrated within the CIP-II region (Fig. 6*C*). Mouse IP_5 2-K presents a long and flexible loop (Ser272-Gly316, 45 residues) that crosses back the whole CIP (Fig. 5 and 6*C*). Interestingly, this loop is the one that provides a cysteine residue (Cys291) that completes the Zn1 site present in *m*IP_5 2-K (Fig. 4). In addition, this loop seems to stabilize the protein, since it packs with several regions of the enzyme, including both lobes, but mainly the CIP-lobe. In particular, it makes hydrogen bonds through four residues (Leu283, Arg289, Glu292 and Ser294), and shows strong hydrophobic interactions through seven residues (Leu281, Leu283, Pro288, Ala293, Pro295, Leu313, Pro314) (Fig. 6*E*). These residues are fully or highly conserved along the mammal isoforms. Only residues Leu283 and Arg289 show a great variation, both involved in hydrogen bonds through their main chain atoms with other parts of the protein (Fig. 6*E*). Finally, a third difference (D3) is shown in a region also located in the CIP-II (Fig. 6*D*). Precisely, *At*IP_5 2-K presents a zinc site located in this region (25) that is shorter than and completely different from that found in *m*IP_5 2-K (Fig. 6*C* and 6*D*).

Noticeably, different regions of the two isoforms seem to share roles. On one hand, D1 and D3, from *At*IP_5 2-K and *m*IP_5 2-K respectively (Fig. 6*B* and 6*D*), are both stabilizing essential zones of the enzyme, as are α1 (Asn54-Phe66, analogous to protein kinases αC) and other CIP residues. Some relevant interactions of these regions are shown in Fig. 6*F* and 6*G*. Among them, it is worth to mention the central role of Tyr363, Phe367 and Tyr368 in *m*IP_5 2-K (Fig. 6*F*), residues absolutely conserved in the mammal IP5 2-K isoforms. *At*IP_5 2-K presents residues with similar role to Tyr363 (Leu75) and Phe367 (Trp69) that interact with equivalent regions of the protein (Fig. 6*G*). We have selected residue Tyr363 for mutation, since it seems key in the network of interactions as proposed above. Y363A mutation halves enzymatic activity (Fig. 6*H*). Unexpectedly, this decrease in activity is moderate. An explanation is that it corresponds to a single mutation among a multiple net of interactions and in a residue far from the active site. On the other hand, *m*IP_5 2-K D2 and *At*IP_5 2-K D3 (Fig. 6*C* and 6*D*) are both involved in generation of the Zinc Sites which are not conserved either in sequence, location or structure between both enzymes. However, both sites seem to have a structural role, although we cannot discard any other additional function. Strikingly, the insertions found in *m*IP_5 2-K (D2 and D3) interact with each other (Fig. 6*E*). Thus, Tyr368 in

mIP_5 2-K and the following leucine residues (Leu372 and Leu374) interact with Leu281 and Leu283 located in D2 (Fig. 6*E*). A double mutation in this region (L281A/L283A) reduces slightly the activity in contrast with the >90% decreases caused by the other mentioned mutation on a zinc binding residue (C291S) within this segment (Fig. 6*H*). All the mentioned leucine residues show very high conservation, except Leu283 as mentioned previously. A mutation in this residue would keep the capacity of making hydrogen bonds through its main chain (Fig. 6*E*) and the slight structural destabilization introduced has no impact in the protein active site.

Novel findings in mammal IP_5 2-K substrates binding and catalysis-Most residues involved in substrate binding and catalysis are conserved between mammal and plant IP_5 2-Ks (Fig. 5). Nevertheless, we can observe some differences in the inositide P1 and P3 coordination. As shown, inositide P1 interacts extensively with Arg100 of *m*IP_5 2-K (Fig. 2*C*). The role of the Arg100 equivalent in *At*IP_5 2-K (Arg130) has been largely argued, and an implication in substrate binding and triggering of a productive protein conformation has been proposed (27,29,30). Unfortunately a construct prepared for R100A *m*IP_5 2-K mutant did not show expression in the soluble fraction. However we can conclude that this residue is structurally similar to Arg130 in *At*IP_5 2-K. In *m*IP_5 2-K, additional interactions with P1 are produced through the side chain of Lys173, a residue non-conserved with the plant IP_5 2-Ks but absolutely conserved in mammal enzymes, whereas conservative substitutions can be observed in other vertebrates (Fig. 7). However, mutation of Lys173 produces an enzyme as active as the wild type (Fig. 7*A*) showing very similar kinetic parameters (Fig. 3*A*), suggesting that this interaction is dispensable for substrate binding and it probably might have other implications, as will be commented later.

Inositide P3 coordinates with the main chain of the G-loop in both enzymes, but different additional interactions are made within the two enzymes. In *m*IP_5 2-K, P3 also interacts with the side chains of Asn18 and Lys19 G-loop residues whereas the plant enzyme provides two arginine residues from a different region (Arg45 and Arg415) to complete this binding. Double mutation on the G-loop residues Asn18/Lys19 (Fig. 7*A*) has a notable impact in the enzymatic activity, supporting a main role for these G-loop residues absolutely conserved in mammals (Fig. 7*C*).

We also can observe particular features in catalytic residues in the connecting loops (Fig. 1*B*). We have prepared mutations on relevant residues from these CLs (K138A, D437A and D439A) (Fig. 2*D*), obtaining mutated enzymes with very low activities (Fig. 7*B*). The role of equivalent residues to Lys138 and Asp437 has been largely studied along the PKs and IPK families. These residues are responsible for neutralizing the negative charge developed in the transition state and orienting the nucleotide Pγ through Mg ions respectively. We observe in *m*IP_5 2-K that Asp439 displays a strategic position, helping in Mg coordination and forming a bridge with Arg33, a residue involved in the coordination of nucleotide phosphates. Therefore it seems to provide a proper conformation for essential parts of the enzyme (Fig. 7*B*). No mutagenesis data has been reported on the Asp439 equivalent residues in other enzymes, since an homologous residue in this position is not present (neither in the IPK or PK families). Asp439 shows a notable conservation in the whole IP_5 2-K family across the species (Fig. 7*C*), showing only changes by a serine residue in some plant IP_5 2Ks, which in turn also coordinates the Mg atom (25). We show here that D439A mutation produce nearly inactive enzyme. Finally, the connecting loop CL3 does not show significant conservation between *m*IP_5 2-K and *At*IP_5 2-K, either in length or sequence, This loop is responsible in *At*IP_5 2-K for interactions between N- and C-lobe that might regulate partially the catalysis through opening and closing the active site (27). In addition this loop makes interactions with two residues directly involved in inositide binding, one of them (Arg130) shown to be essential for protein activity (27). We think that differences in this loop may also account for the differences observed in the K_m from each protein. In *m*IP_5 2-K structure, this loop is disordered and therefore interaction with the N-lobe has not been determined (Fig. 1). However, the flexibility found in the *m*IP_5 2-K CL3 loop is consistent with a dynamic role and the previous proposed functions in catalysis regulation.

A prominent basic patch on mIP$_5$ 2-K surface-The structure of *m*IP$_5$ 2-K shows a very notable basic patch on its surface, mainly concentrated down the active site face of the enzyme (Fig. 8*A*). The enzyme regions that contribute to this patch are α6, α8 in CIP-I and the large insert found in CIP-II region. Interestingly, only a few of these basic residues are present or conserved in *At*IP$_5$ 2-K (Fig. 8*B*), which apart from the basic pocket for the inositide binding does not show any significantly accumulation of arginine or lysine residues on its surface. By contrast, most of these residues are conserved across the mammal isoforms. This striking feature could be correlated with mammal IP$_5$ 2-K localization and/or other possible functions that this enzyme could present in cells. Particularly outstanding are two basic segments, one formed by residues Lys 175, Lys176 and Lys 179 and the other containing the residues in the new insert (D2) found in mammals and its preceding helix (Lys255, Arg259, Arg267, Lys275, Lys289 and Lys315). The first segment overlaps in part with the motif ^{173}KW K/R K/Q, highly conserved in mammals. The second segment encloses one of the main differences (D2) found with respect to plant enzymes. Based on the present finding, we propose that this insert, apart from supporting the zinc binding and stabilizing some protein regions, could be delineating a particular protein surface that could serve as an interface for other partners essential for IP$_5$ 2-K function.

DISCUSSION

Herein we described the first structure of a mammal IP$_5$ 2-K, a key enzyme in inositol metabolism with multiple impacts in diverse cellular events. Structural knowledge of this enzyme is essential to fully understand its function, although the fact that mammalian IP$_5$ 2-K shows extremely low bacterial expression and very low tendency to produce suitable crystals has precluded it up to now. The structure of *m*IP$_5$ 2-K presented here shows large structural differences with the *At*IP$_5$ 2-K concentrated in the helical regions. Both enzymes are zinc metalloenzymes, the zinc sites showing different location and structural features. Whereas the plant zinc site is exclusive for its kingdom, the site found in mammals (Zn1) seems to be conserved in all the species except plants. Punctual mutations of the Zn1 ligands present different effects, going from a null protein expression (Cys181) to a decreased zinc amount (Cys291) clearly correlated with a dramatic drop in protein activity and thermal stability. In particular, Cys291, located in a long insertion (D2), is present in all vertebrates and most invertebrates (not shown). This insertion is quite unusual since it is unstructured and placed between two contiguous helices (Fig. 6*C*). Its role seems to support the architecture of the CIP lobe, to complete the zinc binding site and to configure a markedly basic protein surface.

Apart from these remarkable differences found, substrate recognition in both isoforms is quite similar. In previous works, *At*IP$_5$ 2-K was shown to display conformational changes upon substrate binding that set the enzyme lobes together producing a closed conformation (27). Studies performed with *At*IP$_5$ 2-K revealed that the IP$_5$ binding to the C-lobe is stronger, while the binding to the N-lobe is necessary for protein activation and conformational change (30). As the Zn1 is located into the CIP-lobe and far from the N-lobe, we suggest that it would affect the preliminary inositide binding events rather than the subsequent dynamic behavior of the protein. The structure solved for *m*IP$_5$ 2-K probably corresponds to the close conformation in agreement with the fact that the inositide substrate is present in the structure and the good superposition of *m*IP$_5$ 2-K reported here onto the *At*IP$_5$ 2-K closed conformation. We do not know if the changes reported for *At*IP$_5$ 2-K also occur in the mammal isoforms and if they are a general behavior of the IP$_5$ 2–K family. However, the conservation of several elements involved in these changes, as the flexibility of CL3 or inositide binding by N-lobe through Arg100 or G-loop, suggests that this open-close mechanism could be proposed for mammal IP$_5$ 2-Ks. In relation to this, we made proteolysis experiments to check if the substrates protect the enzyme digestion as happened in *At*IP$_5$ 2-K (28). We observed no protection in *m*IP$_5$ 2-K, probably due to the fact that its digestion sites are far from regions involved in the conformational change. Moreover, we did not get crystals in absence of substrates, which could be pointing to some structural changes though this is not conclusive either.

The structure of *At*IP_5 2-K revealed that IP_5 2-Ks are the most divergent among the IPK family, since it has the most elaborated CIP-lobe and binds the substrate in very different orientation to face an axial OH to Pγ of phosphate. Similarly, IP_5 2-Ks are the most divergent enzymes classified inside the PK structural superfamily, what is confirmed in the here presented structure. Moreover, we observe that *m*IP_5 2-K lacks the N-lobe acidic residue (Glu91, PKA nomenclature) reported to salt-bridge to a basic residue (Lys72, PKA nomenclature) and involved in ATP phosphate coordination. This bridge is a hallmark that identifies the protein kinases active conformation, and equivalent residues are also present in other IPKs. In contrast, *m*IP_5 2-K has a different acidic residue, Asp439, which stabilizes Arg33 (equivalent to Lys72 in PKAs). Therefore, in IP_5 2-K family this bridge could play a similar role to that described in PKs.

Brehm and co-workers have investigated the human IP_5 2-K and, in particular, the possibility of additional functions apart from its catalytic role (12,13). They found that *h*IP_5 2-K colocalizes with mRNA, both in the nuclei and cytoplasm. (13). The mutations on a region rich in basic residues, coincident with the ^{173}KW K/R K/Q motif conserved in mammals, shows an altered enzyme ability to be exported out of the nuclei. This regions is exposed and included within the basic patch of *m*IP_5 2-K identified in this work (Fig. 7*C* and 8). Interestingly, Lys173 at the beginning of the above motif coordinates the inositide substrate. However our mutagenesis experiments showed that this residue is dispensable for substrate binding, suggesting that the major role for this motif is played in the translocation process proposed by Brehm et al. (13). In addition, *h*IP_5 2-K was shown to be a structural component of the nucleolus acting as a molecular scaffold in nucleoli and influencing the degree of rRNA synthesis, therefore having a role in rRNA biogenesis. In relation to this, *h*IP_5 2-K interacts with three proteins (CK2, TCOF and UBF) that regulate rRNA synthesis. In particular, UBF interacts with a basic region (^{41}RKK motif equivalent to ^{41}KKK motif in *m*IP_5 2-K) (12) its mutation preventing the UBF translocation out of nucleolus after *h*IP_5 2-K overexpression. As the authors predict, this region is completely exposed, and we observe that it is in a flexible loop as shown by its poor electron density. We now disclose the high and specific basic region found in mammal IP_5 2-Ks surface that could be used as a guide to find more target points.

In conclusion, our work provides novel features for the IP_5 2-Ks family and its mammal isoforms. Unexpected protein regions and residues have been identified providing an illuminating picture of these enzymes. The findings comprise the characterization of subtle but important features for substrate recognition, including unreported catalytic residues for this family, the identification of an unusual and exclusive zinc binding site and the conspicuous basic patch on the protein surface. Undoubtedly, the results obtained in this work provide a valuable tool for the design of therapeutics targeted at mammalian IP_5 2-K with potential implications in health and also to perform IP_5 2-K functional studies. Beyond catalytic function, our work also suggests putative regions of interaction of mammalian IP_5 2-Ks with the cognate partners necessary to accomplish their precise functions.

EXPERIMENTAL PROCEDURES

Protein expression and purification- Constructs for full length IP_5 2-K recombinant expression either in bacteria (m*ipk1*/pKLSLt plasmid) or insect cells were obtained as described by us (34) from a m*ipk1* cDNA (commercial clone bc062167). In order to produce a truncated *m*IP_5 2-K enzyme lacking the 21 C-terminal residues (ΔC-*m*IP_5 2-K) a stop codon was introduced at position coding for residue 469 of *m*IP_5 2-K by site directed mutagenesis and using as template the m*ipk1* cDNA inserted into pKLSLt vector (35). Punctual and double ΔC-*m*IP_5 2-K mutants were obtained by site directed mutagenesis using as template the ΔC-m*ipk1*/pKLSLt plasmid. Primers used for construct preparations are shown in Table S3.

Expression and purification of ΔC-*m*IP_5 2-K samples fused to LSL- was performed similarly to the full-length samples (34). Briefly, the protein was expressed in *E. coli* BL21 Star (DE3) cells in 2TY medium supplemented with kanamycin (50 μg ml $^{-1}$) at 310 K until an OD_{600} of 0.9 was reached. Expression was induced with 0.3 mM IPTG for 96 h at 283 K. Pellets were resuspended and sonicated in buffer A (20 mM Tris–HCl pH 8.0, 150 mM NaCl, 1 mM DTT) plus 0.2 mM PMSF and 0.05% Triton X-100. The filtrated

lysate was diluted 3-fold, loaded onto an heparin column, washed with buffer B (20 mM Tris HCl pH 8, 50 mM NaCl, 1 mM DTT) and eluted with a 1M NaCl gradient. The fusion protein was applied onto a Sepharose CL-6B column equilibrated in buffer A and eluted using 200 mM lactose, followed by o/n cleavage with TEV protease (protease: protein mass ratio 1: 40) gently rolling at 278 K. Our protein was separated from LSLt and TEV protease by a second heparin column and further purified by size-exclusion chromatography (HiLoad 16/600 Superdex 200 column) equilibrated in buffer A plus 2mM IP_6, which was included to avoid protein precipitation. All *m*IP_5 2-K samples used for crystallization were concentrated to around 5-6 mg ml $^{-1}$ and stored at 193 K. We obtained 1 mg of pure ΔC-*m*IP_5 2-K per litre of bacteria culture. The purity of all the samples was confirmed by SDS–PAGE. For crystallization and CD analysis, WT and C291S ΔC-IP_5 2-K samples were purified using this protocol.

Finally, for activity assays, wild type LSLt-ΔC-*m*IP_5 2-K and mutants were purified as following. Clarified and filtrated cell lysate in buffer A was applied to a Sepharose CL-6B column equilibrated in buffer A. After washing with buffer A, the protein was eluted with 200 mM lactose. The sample was diluted 3-fold with 20 mM Tris HCl pH 8.0, loaded onto an heparin column and washed with buffer B and eluted with a salt gradient. The protein in final buffer C (20 mM Tris HCl pH 8.0, 700 mM NaCl, 1mM DTT) was concentrated to 1-3 mg ml $^{-1}$ and stored at −80 °C.

Crystallization-All IP_5 2-K samples used for crystallization were obtained in presence of 2mM IP_6. Best crystals obtained for the full-length *m*IP_5 2-K expressed either in bacteria or in insect cells diffracted to 4-4.3 Å (34), which did not allowed the structure solution. Finally, ΔC-*m*IP_5 2-K construct allowed us to improve resolution to 3.2 Å from crystals grown in 0.2 M magnesium chloride, 0.1 M MES pH 6.25, 10% (v/v) PEG 6000 and including 2 mM IP_6 and 2 mM ADP in the protein buffer. A new pH grid screen using the sample in presence of 2mM IP_6 allowed us to get better crystals grown in 0.2 M magnesium chloride, 0.1 M sodium acetate pH 5.5, 16% (v/v) PEG 6000. Soaking experiments in precipitant solutions containing 10 mM IP_6 or 10 mM IP_6/ADP during 3 hours yielded the complexes *m*IP_5 2-K/IP_6 and *m*IP_5 2-K/IP_5/ATP diffracting to 2.4 Å in the last case. Microseeding technique was necessary to improve the quality of all these crystals. For this purpose, we selected our best crystals and introduced them into 50 µl of crystallization solution plus a seeding bead. After two cycles of 30 s vortex and 30 s on ice, we made a seed stock. We streak-seed the crystallization drops with a whisker using this seed stock. All IP_5 2-K crystals appeared in a few hours after setting up the crystallization trials, and we observed that the protein is degraded in the crystallization conditions very quickly making crystal optimization extremely difficult.

Data collection and structural determination- Crystals were transferred for a few seconds into precipitant solution plus 20% (v/v) glycerol and then flash-cooled in liquid nitrogen. Data from IP_5 2-K crystals were collected at 100 K in beam line BL13-XALOC of ALBA synchrotron (36). ΔC-mIP_5 2-K crystallizes in monoclinic $P2_1$ space group in two different forms having one (pH 5.5) or two molecules (pH 6.25) in the asymmetric unit (Table 1). Diffraction data were indexed, integrated and scaled using XDS (37) and merged using Aimless (38) from CCP4 suite (39,40). Initially, ΔC-*m*IP_5 2-K monoclinic crystals grown at pH 6.5 (3.2 Å) allowed us to get a partial model using molecular replacement with MOLREP (41) and the structure of *A. thaliana* IP_5 2-K as a search model (PDB code 2XAN). However the preliminary electron density maps presented many ambiguities, though clearly showed high positive difference peaks for two possible zinc ions. An anomalous map computed with PHENIX (42) showed a strong anomalous signal in those positions (Fig. S2). Therefore we tried SAD phasing in combination with MR (MRSAD-Auto-Rickshaw) (43). The heavy atoms positions were located using PHASER (44) and refined with MLPHARE (39). The phases obtained were then combined and density modification was performed with RESOLVE (45,46) and PIRATE (47). Final electron density maps allowed the building of the whole chain except some exposed loops indicating the flexibility of these regions.

Later, the ΔC-*m*IP_5 2-K monoclinic crystals grown at pH 5.5 allowed us to refine the

structure of protein complexes with ligands IP_6 and IP_5/ATP to 2.6 Å and 2.4 Å maximum resolution, respectively. The structures were solved by molecular replacement using MOLREP (41) and the coordinates of ΔC-*m*IP_5 2-K described above as a search model. The substrates/products were manually fit into the electron density maps. Although we soaked the crystals with the products IP_6/ADP, the initial electron density maps showed clear density consistent with IP_5 and ATP (Fig. S1). Then, we checked that our crystallized *m*IP_5 2-K samples are able to catalyze both the forward and reverse reactions in solution (Fig. 3*B* and *C*) and, therefore, we modeled the substrates IP_5/ATP in the active site. Model refinement was performed with REFMAC (48) alternating with manual model building using COOT (49). The stereochemistry of the model have been checked with PROCHECK (50). Statistics for all data processing and refinement are summarized in Table 1. Figures of the models were generated with PYMOL (51).

Circular dichroism-CD spectra were recorded using a Jasco-810 spectropolarimeter equipped with a Peltier-thermostatted cell holder. Measurements in the Far-UV region (250-200 nm) were performed using the samples WT and C291S ΔC-IP_5 2-K after protein buffer exchange to 25 mM sodium phosphate pH 8 and at protein concentrations of 0.1 mg ml^{-1} (10 mm path-length quartz cells; bandwidth, 1 nm; response, 4 s; scan speed 20 nm min^{-1}). Collected spectra were the average of four accumulations. The data were converted to molar ellipticities after subtraction of the buffer contribution using the average molecular mass per residue (114 Da). Thermal denaturation was monitored by CD measuring the ellipticity changes at 220 nm as the temperature was raised (20-90 ^{o}C) at 60 ^{o}C h^{-1}. The normalized ellipticity value at each temperature was calculated as ([θ]t – [θ]25)/([θ]90 – [θ]25), where [θ]t is the ellipticity value at temperature t, and [θ]25 and [θ]90 are the ellipticity values at 25 °C and 90 °C, respectively.

Protein sequence alignments and bioinformatics-IP_5 2-Ks sequences of all kingdoms have been retrieved using BLAST (https://blast.ncbi.nlm.nih.gov/Blast.cgi) and Pfam (52) searches. After removing all incomplete sequences or lacking essential hallmarks for kinase function, we had a collection of the following sequences: 102 for mammals, 142 for non mammal vertebrates, 28 for invertebrates, 158 for fungi and 203 for plants. Sequence alignments have been performed with CLUSTAL omega server (53) and corrected manually with SeaView (54). A structural alignment between *At*IP_5 2-K (code 1xan) and *m*IP_5 2-K has been performed with EPSPRIT (55)

Enzyme assays-LSL-ΔC-IP_5 2-K and ΔC-IP_5 2-K samples showed comparable activity (not shown); therefore we used LSL tagged samples for analysis of kinetic parameters of WT and mutants. For this purpose, IP_5-dependent conversion of ATP to ADP was determined by HPLC. Assays were performed in 20 mM Hepes, 1 mM $MgCl_2$, pH 7.3 containing 0.2 – 5 µM Ins(1,3,4,5,6)P_5 and 50 µM ATP in a volume of 50-100 µl at an enzyme concentration of 4 µg ml^{-1}. Reactions were stopped by the addition of 50 µl of 60 mM $(NH_4)_2HPO_4$, pH 3.8 with H_3PO_4. Aliquots of the reaction products were resolved by ion-pair reverse phase chromatography (56) with the following modifications: separations were performed on a 100 mm x 2.1 mm Agilent X-Bridge C18 (3.5 µm particle size) column eluted at a flow rate of 0.25 ml min^{-1}. Nucleotide substrates and products (ADP and ATP) were detected at 260 nm and the extent of conversion of one to the other determined from the ratio of integrated peaks. The ADP content of the ATP used was less than 0.1% of the ATP peak area. Reaction velocities were calculated assuming 1:1 stoichiometry of consumption of nucleotide and inositide. Experimental data were fitted by non-linear least squares regression to the Michaelis-Menten equation in GraFit (Erithacus Software). Assays were performed in triplicate and the experiment repeated an additional 3 times with similar results.

Verification of reactions catalyzed by mIP_5 2-K-We undertook a variety of enzyme assays to determine the identities of products formed by the enzyme. We tested the ability of ΔC-*m*IP_5 2-K to catalyze forward 'kinase' and reverse reactions.

For the forward 'kinase' reaction, 2.4 µg of ΔC-*m*IP_5 2-K was incubated with 200 µl of 100

μM Ins(1,3,4,5,6)P_5 (sodium salt, SiChem, Germany), 40 μM ATP in 20 mM Hepes, 1 mM $MgCl_2$, pH 7.3 at 37°C. At intervals, aliquots were withdrawn and 20 μL injected onto a 250 mm x 3 mm CarboPac PA200 column (Dionex) eluted at a flow rate of 0.4 ml min^{-1} with a gradient derived from buffer reservoirs containing: A, water; B 0.6 M methanesulfonic acid according to the following profile: time (min), % B; 0, 0; 25, 100; 38, 100. The eluate from the column was mixed in a mixing tee with colour-reagent (0.1 % w/v $Fe(NO_3)_3.9H_2O$ in 2% v/v $HClO_4$, after (57) delivered at a flow rate of 0.2 ml min^{-1} by a second hplc pump. The combined flow was monitored at 290 nm after passage through a knitted reaction coil.

For the reverse reaction, 2.4 μg of ΔC-*m*IP_5 2-K was incubated with 200 μl of 100μM IP_6 (sodium salt, Merck, Germany), 50 μM ADP in 20 mM Hepes, 1 mM $MgCl_2$, pH 7.3 at 37°C, with subsequent processing as above. The identity of IP_5 and IP_6 products was confirmed by chromatography of standards (SiChem or Merck) and by analysis of an IP_6 hydrolyzate obtained by overnight refluxing of IP_6 in 1M-HCl, with subsequent rotary evaporation to remove HCl.

Our Ins(1,3,4,5,6)P_5 [IP_5 2-OH] substrate contained D- and/or L-Ins(1,2,4,5,6)P_5 [IP_5 1/3-OH], but our analysis which resolves the two *meso*-compounds (IP_5 2-OH and IP_5 5-OH) from the two pairs of enantiomers (IP_5 1/3-OH and IP_5 4/6-OH) confirmed that *m*IP_5 2-K is an inositol 1,3,4,5,6-pentakisphosphate 2-kinase that does not accept D- and/or L-Ins(1,2,4,5,6)P_5 (mixture unknown) as substrate (Fig. 3*B*). HPLC traces were exported from Jasco (Great Dunmow, UK) ChromNav software as asci files and redrawn in GraFit (Erithacus Software).

Inductively Coupled Plasma-Optical Emission Spectroscopy-Metal analysis of *m*IP_5 2-K was performed by optical emission spectroscopy on a Varian Vista Pro ICP-OES. Protein or buffer in which protein was prepared were diluted 125-139 fold in 18.2 MOhm.cm water containing 1N HNO_3. Diluted protein or buffer were subjected to ICP-OES on a machine calibrated with 0–4.0 μM standards of Co, Cu, Ni, and Zn in 1N HNO_3. All metals except zinc were close to the limit of detection in the diluted protein sample; they were only slightly above the background in the buffer (Table S2).

Acknowledgments: Data collection was performed at XALOC-BL13 beamline at ALBA Synchrotron with the collaboration of ALBA staff. We thank Graham Chilvers, UEA SCI Faculty Analytical Facility, for assistance with ICP-OES. The authors acknowledge the support and the use of resources of the French Infrastructure for Integrated Structural Biology FRISBI ANR-10-INSB-05 and of Instruct, a Landmark ESFRI project. C.A.B. was supported by the Biotechnology and Biological Sciences Research Council (UK) by grants BB/N002024/1 and BB/M022978/1. This work and E.F.-E have been supported by Grants BFU2011-24982 and BFU2014-53762-P from the Spanish Ministry of Economy and Competitiveness.

Conflict of interest: The authors declare that they have no conflicts of interest with the contents of this article.

Author contributions: E.F.-E and J.M.G. prepared the constructs for the experiments. E.F.-E expressed, purified and crystallized all the protein samples. E.F.-E and B.G. solved the protein structures. E.F.-E, J.S-A and B.G. analyzed the structural data. C.A.B. performed all enzyme assays and Zinc measurements. J.S-A participated in work and results discussion. B.G. designed research and wrote the paper. All authors edited the manuscript.

REFERENCES

1. Stephens, L. R., Hawkins, P. T., Stanley, A. F., Moore, T., Poyner, D. R., Morris, P. J., Hanley, M. R., Kay, R. R., and Irvine, R. F. (1991) myo-inositol pentakisphosphates. Structure, biological occurrence and phosphorylation to myo-inositol hexakisphosphate. *Biochem. J.* **275 (Pt 2)**, 485-499

2. Shears, S. B. (2001) Assessing the omnipotence of inositol hexakisphosphate. *Cell. Signalling* **13**, 151-158
3. Ouyang, Z., Zheng, G., Tomchick, D. R., Luo, X., and Yu, H. (2016) Structural Basis and IP6 Requirement for Pds5-Dependent Cohesin Dynamics. *Mol. Cell* **62**, 248-259
4. Alcazar-Roman, A. R., Tran, E. J., Guo, S., and Wente, S. R. (2006) Inositol hexakisphosphate and Gle1 activate the DEAD-box protein Dbp5 for nuclear mRNA export. *Nat. Cell. Biol.* **8**, 711-716
5. Macbeth, M. R., Schubert, H. L., Vandemark, A. P., Lingam, A. T., Hill, C. P., and Bass, B. L. (2005) Inositol hexakisphosphate is bound in the ADAR2 core and required for RNA editing. *Science* **309**, 1534-1539
6. Boularan, C., Scott, M. G., Bourougaa, K., Bellal, M., Esteve, E., Thuret, A., Benmerah, A., Tramier, M., Coppey-Moisan, M., Labbe-Jullie, C., Fahraeus, R., and Marullo, S. (2007) beta-arrestin 2 oligomerization controls the Mdm2-dependent inhibition of p53. *Proc. Nat. Acad. Sci. U.S.A.* **104**, 18061-18066
7. Scherer, P. C., Ding, Y., Liu, Z., Xu, J., Mao, H., Barrow, J. C., Wei, N., Zheng, N., Snyder, S. H., and Rao, F. (2016) Inositol hexakisphosphate (IP6) generated by IP5K mediates cullin-COP9 signalosome interactions and CRL function. *Proc. Nat. Acad. Sci. U.S.A.* **113**, 3503-3508
8. Byrum, J., Jordan, S., Safrany, S. T., and Rodgers, W. (2004) Visualization of inositol phosphate-dependent mobility of Ku: depletion of the DNA-PK cofactor InsP6 inhibits Ku mobility. *Nucleic Acids Res.***32**, 2776-2784
9. Barker, C. J., Illies, C., Gaboardi, G. C., and Berggren, P. O. (2009) Inositol pyrophosphates: structure, enzymology and function. *Cell. Mol. Life Sci.* **66**, 3851-3871
10. Chakraborty, A., Koldobskiy, M. A., Sixt, K. M., Juluri, K. R., Mustafa, A. K., Snowman, A. M., van Rossum, D. B., Patterson, R. L., and Snyder, S. H. (2008) HSP90 regulates cell survival via inositol hexakisphosphate kinase-2. *Proc. Nat. Acad. Sci. U.S.A.* **105**, 1134-1139
11. Verbsky, J., Lavine, K., and Majerus, P. W. (2005) Disruption of the mouse inositol 1,3,4,5,6-pentakisphosphate 2-kinase gene, associated lethality, and tissue distribution of 2-kinase expression. *Proc. Nat. Acad. Sci. U.S.A.* **102**, 8448-8453
12. Brehm, M. A., Wundenberg, T., Williams, J., Mayr, G. W., and Shears, S. B. (2013) A non-catalytic role for inositol 1,3,4,5,6-pentakisphosphate 2-kinase in the synthesis of ribosomal RNA. *J. Cell Sci.* **126**, 437-444
13. Brehm, M. A., Schenk, T. M., Zhou, X., Fanick, W., Lin, H., Windhorst, S., Nalaskowski, M. M., Kobras, M., Shears, S. B., and Mayr, G. W. (2007) Intracellular localization of human Ins(1,3,4,5,6)P5 2-kinase. *Biochem. J.* **408**, 335-345
14. Berridge, M. J., and Irvine, R. F. (1984) Inositol trisphosphate, a novel second messenger in cellular signal transduction. *Nature* **312**, 315-321
15. Wang, H., Falck, J. R., Hall, T. M., and Shears, S. B. (2011) Structural basis for an inositol pyrophosphate kinase surmounting phosphate crowding. *Nat. Chem. Biol.* **8**, 111-116
16. Qian, X., Mitchell, J., Wei, S. J., Williams, J., Petrovich, R. M., and Shears, S. B. (2005) The Ins(1,3,4)P3 5/6-kinase/Ins(3,4,5,6)P4 1-kinase is not a protein kinase. *Biochem. J.* **389**, 389-395
17. Onnebo, S. M., and Saiardi, A. (2007) Inositol pyrophosphates get the vip1 treatment. *Cell* **129**, 647-649
18. Saiardi, A., Caffrey, J. J., Snyder, S. H., and Shears, S. B. (2000) The inositol hexakisphosphate kinase family. Catalytic flexibility and function in yeast vacuole biogenesis. *J. Biol. Chem.* **275**, 24686-24692
19. Shears, S. B. (2004) How versatile are inositol phosphate kinases? *Biochem. J.* **377**, 265-280
20. Phillippy, B. Q., Ullah, A. H., and Ehrlich, K. C. (1994) Purification and some properties of inositol 1,3,4,5,6-Pentakisphosphate 2-kinase from immature soybean seeds. *J. Biol. Chem.* **269**, 28393-28399

21. Irvine, R. F., Letcher, A. J., Heslop, J. P., and Berridge, M. J. (1986) The inositol tris/tetrakisphosphate pathway--demonstration of Ins(1,4,5)P3 3-kinase activity in animal tissues. *Nature* **320**, 631-634
22. Cheek, S., Zhang, H., and Grishin, N. V. (2002) Sequence and structure classification of kinases. *J. Mol. Biol.* **320**, 855-881
23. Gonzalez, B., Schell, M. J., Letcher, A. J., Veprintsev, D. B., Irvine, R. F., and Williams, R. L. (2004) Structure of a human inositol 1,4,5-trisphosphate 3-kinase: substrate binding reveals why it is not a phosphoinositide 3-kinase. *Mol. Cell* **15**, 689-701
24. Wang, H., DeRose, E. F., London, R. E., and Shears, S. B. (2014) IP6K structure and the molecular determinants of catalytic specificity in an inositol phosphate kinase family. *Nat. Commun.* **5**, 4178
25. Gonzalez, B., Baños-Sanz, J. I., Villate, M., Brearley, C. A., and Sanz-Aparicio, J. (2010) Inositol 1,3,4,5,6-pentakisphosphate 2-kinase is a distant IPK member with a singular inositide binding site for axial 2-OH recognition. *Proc. Nat. Acad. Sci. U.S.A.* **107**, 9608-9613
26. Holmes, W., and Jogl, G. (2006) Crystal structure of inositol phosphate multikinase 2 and implications for substrate specificity. *J. Biol. Chem.* **281**, 38109-38116
27. Baños-Sanz, J. I., Sanz-Aparicio, J., Whitfield, H., Hamilton, C., Brearley, C. A., and Gonzalez, B. (2012) Conformational changes in inositol 1,3,4,5,6-pentakisphosphate 2-kinase upon substrate binding: role of N-terminal lobe and enantiomeric substrate preference. *J. Biol. Chem.* **287**, 29237-29249
28. Gosein, V., Leung, T. F., Krajden, O., and Miller, G. J. (2012) Inositol phosphate-induced stabilization of inositol 1,3,4,5,6-pentakisphosphate 2-kinase and its role in substrate specificity. *Protein Sci.* **21**, 737-742
29. Gosein, V., and Miller, G. J. (2013) Conformational stability of inositol 1,3,4,5,6-pentakisphosphate 2-kinase (IPK1) dictates its substrate selectivity. *J. Biol. Chem.* **288**, 36788-36795
30. Gosein, V., and Miller, G. J. (2013) Roles of phosphate recognition in inositol 1,3,4,5,6-pentakisphosphate 2-kinase (IPK1) substrate binding and activation. *J. Biol. Chem.* **288**, 26908-26913
31. Verbsky, J. W., Wilson, M. P., Kisseleva, M. V., Majerus, P. W., and Wente, S. R. (2002) The synthesis of inositol hexakisphosphate. Characterization of human inositol 1,3,4,5,6-pentakisphosphate 2-kinase. *J. Biol. Chem.* **277**, 31857-31862
32. Sweetman, D., Johnson, S., Caddick, S. E., Hanke, D. E., and Brearley, C. A. (2006) Characterization of an Arabidopsis inositol 1,3,4,5,6-pentakisphosphate 2-kinase (AtIPK1). *Biochem. J.* **394**, 95-103
33. Holm, L., and Rosenstrom, P. (2010) Dali server: conservation mapping in 3D. *Nucleic Acids Res.* **38**, W545-549
34. Franco-Echevarria, E., Sanz-Aparicio, J., Troffer-Charlier, N., Poterszman, A., and Gonzalez, B. (2017) Crystallization and Preliminary X-Ray Diffraction Analysis of a Mammal Inositol 1,3,4,5,6-Pentakisphosphate 2-Kinase. *Protein J* DOI: 10.1007/s10930-017-9717-y
35. Angulo, I., Acebron, I., de las Rivas, B., Munoz, R., Rodriguez-Crespo, I., Menendez, M., Garcia, P., Tateno, H., Goldstein, I. J., Perez-Agote, B., and Mancheno, J. M. (2011) High-resolution structural insights on the sugar-recognition and fusion tag properties of a versatile beta-trefoil lectin domain from the mushroom Laetiporus sulphureus. *Glycobiology* **21**, 1349-1361
36. Juanhuix, J., Gil-Ortiz, F., Cuni, G., Colldelram, C., Nicolas, J., Lidon, J., Boter, E., Ruget, C., Ferrer, S., and Benach, J. (2014) Developments in optics and performance at BL13-XALOC, the macromolecular crystallography beamline at the ALBA synchrotron. *J. Synchrotron Radiat.* **21**, 679-689
37. Kabsch, W. (2010) Xds. *Acta Crystallogr D Biol Crystallogr* **66**, 125-132
38. Evans, P. R. (2011) An introduction to data reduction: space-group determination, scaling and intensity statistics. *Acta Crystallogr D Biol Crystallogr* **67**, 282-292

39. The CCP4 (Collaborative Computational Project, n. (1994) The CCP4 suite: programs for protein crystallography. *Acta Crystallogr D Biol Crystallogr* **50**, 760-763
40. Winn, M. D., Ballard, C. C., Cowtan, K. D., Dodson, E. J., Emsley, P., Evans, P. R., Keegan, R. M., Krissinel, E. B., Leslie, A. G., McCoy, A., McNicholas, S. J., Murshudov, G. N., Pannu, N. S., Potterton, E. A., Powell, H. R., Read, R. J., Vagin, A., and Wilson, K. S. (2011) Overview of the CCP4 suite and current developments. *Acta Crystallogr D Biol Crystallogr* **67**, 235-242
41. Vagin, A., and Teplyakov, A. (2010) Molecular replacement with MOLREP. *Acta Crystallogr D Biol Crystallogr* **66**, 22-25
42. Afonine, P. V., Grosse-Kunstleve, R. W., Echols, N., Headd, J. J., Moriarty, N. W., Mustyakimov, M., Terwilliger, T. C., Urzhumtsev, A., Zwart, P. H., and Adams, P. D. (2012) Towards automated crystallographic structure refinement with phenix.refine. *Acta Crystallogr D Biol Crystallogr* **68**, 352-367
43. Panjikar, S., Parthasarathy, V., Lamzin, V. S., Weiss, M. S., and Tucker, P. A. (2009) On the combination of molecular replacement and single-wavelength anomalous diffraction phasing for automated structure determination. *Acta Crystallogr D Biol Crystallogr* **65**, 1089-1097
44. McCoy, A. J., Grosse-Kunstleve, R. W., Adams, P. D., Winn, M. D., Storoni, L. C., and Read, R. J. (2007) Phaser crystallographic software. *J. Appl. Crystallogr.* **40**, 658-674
45. Terwilliger, T. C. (1999) Reciprocal-space solvent flattening. *Acta Crystallogr D Biol Crystallogr* **55**, 1863-1871
46. Terwilliger, T. C. (2000) Maximum-likelihood density modification. *Acta Crystallogr D Biol Crystallogr* **56**, 965-972
47. Cowtan, K. (2000) General quadratic functions in real and reciprocal space and their application to likelihood phasing. *Acta Crystallogr D Biol Crystallogr* **56**, 1612-1621
48. Murshudov, G. N., Vagin, A. A., and Dodson, E. J. (1997) Refinement of macromolecular structures by the maximum-likelihood method. *Acta Crystallogr D Biol Crystallogr* **53**, 240-255
49. Emsley, P., Lohkamp, B., Scott, W. G., and Cowtan, K. (2010) Features and development of Coot. *Acta Crystallogr D Biol Crystallogr* **66**, 486-501
50. Laskowski RA., M. M. W., Moss DS, Thornton J M. (1993) PROCHECK: a program to check the stereochemical quality of protein structres. *J. Appl. Crystallogr.* **26**, 283-291
51. DeLano, W. L. (2002) The PyMOL Molecular Graphics System. *DELano Scientific LLc, San Carlos, CA*
52. Finn, R. D., Coggill, P., Eberhardt, R. Y., Eddy, S. R., Mistry, J., Mitchell, A. L., Potter, S. C., Punta, M., Qureshi, M., Sangrador-Vegas, A., Salazar, G. A., Tate, J., and Bateman, A. (2016) The Pfam protein families database: towards a more sustainable future. *Nucleic Acids Res.***44**, D279-285
53. Li, W., Cowley, A., Uludag, M., Gur, T., McWilliam, H., Squizzato, S., Park, Y. M., Buso, N., and Lopez, R. (2015) The EMBL-EBI bioinformatics web and programmatic tools framework. *Nucleic Acids Res.***43**, W580-584
54. Gouy, M., Guindon, S., and Gascuel, O. (2010) SeaView version 4: A multiplatform graphical user interface for sequence alignment and phylogenetic tree building. *Mol. Biol. Evol* **27**, 221-224
55. Gouet, P., Robert, X., and Courcelle, E. (2003) ESPript/ENDscript: Extracting and rendering sequence and 3D information from atomic structures of proteins. *Nucleic Acids Res.***31**, 3320-3323
56. Caddick, S. E., Harrison, C. J., Stavridou, I., Mitchell, J. L., Hemmings, A. M., and Brearley, C. A. (2008) A Solanum tuberosum inositol phosphate kinase (StITPK1) displaying inositol phosphate-inositol phosphate and inositol phosphate-ADP phosphotransferase activities. *FEBS lett.* **582**, 1731-1737
57. Phillippy, B. Q., and Bland, J. M. (1988) Gradient ion chromatography of inositol phosphates. *Anal. Biochem.* **175**, 162-166

Footnotes: The atomic coordinates and structure factors have been deposited in the PDB under the following codes: 5MW8, 5MWL and 5MWM.

The abbreviations used are: IP, Inositol phosphate; IP_5, Inositol 1,3,4,5,6-pentakisphosphate; IP_5 2-K, Inositol 1,3,4,5,6-pentakisphosphate 2-kinase; IP_6, Inositol hexakisphosphate; IPK, Inositol polyphosphate kinase; LSL, Laetiporus sulphurous lectin; PEG, Polyethylene glycol; PMSF, Phenylmethanesulfonyl-fluoride; TEV, Tobacco Etch Virus; CK2, protein kinase CK2; TCOF1, treacle protein; UBF, upstream binding factor.

Supplemental data includes Figure S1 and S2 and Tables S1-S3.

Table 1. Crystallographic data statistics and refinement

	ΔC-mIP$_5$ 2-K	**ΔC-mIP$_5$ 2-K**	**ΔC-mIP$_5$ 2-K**
Ligand modeled	+IP$_5$ + ATP	+IP$_6$	+ IP$_5$ +ATP
Crystallization pH	6,25	5,50	5,50
Data collection and processing			
Space group	P 2$_1$	P 2$_1$	P 2$_1$
Unit Cell *a, b, c* (Å)	64.62, 140.76, 68.66	60.55, 71.64, 61.82	60.16, 71.50, 61.20
Unit Cell α, β, γ (Å)	90.0, 106.5, 90.0	90.0, 111.7, 90.0	90.0, 111.4, 90.0
Temperature (K)	100	100	100
Radiation source	Synchrotron	Synchrotron	Synchrotron
Wavelength (Å)	0.979490	0.979260	0.979260
Resolution range (Å)	49.86 - 3.20 (3.42 - 3.20)	44.82 - 2.54 (2.65 - 2.54)	71.50 - 2.40 (2.49 - 2.40)
Nº observed reflections	134008 (24350)	106382 (13008)	123314 (13608)
Nº Unique reflections	19318 (3482)	16270 (1970)	18528 (1961)
Multiplicity	6.9 (7.0)	6.5 (6.6)	6.7 (6.9)
Data completeness (%)	99.3 (99.0)	99.6 (99.7)	97.3 (99.8)
Matthews coef. (Å^3 Da^{-1})	2.32	2.32	2.30
Nº of molecules in a.u.	2	1	1
Wilson B factor (Å ^{2})	83.26	54.65	45.72
Mean I/σ (I)	14.7 (3.3)	12.5 (3.1)	14.9 (3.5)
*R*merge (%) †	10.4 (63.5)	7.6 (58.8)	7.3 (52.8)
*R*pim (%) ††	4.3 (25.8)	3.2 (24.6)	3.1 (21.5)
CC1/2	0.99 (0.89)	0.99 (0.99)	0.99 (0.97)
Refinement			
Resolution range (Å)	70.37 - 3.20	57.45 - 2.60	56.99 - 2.40
*R*work / *R*free††† (%)	22.51/ 24.53	25.34/ 28.95	24.10/ 27.12
Nº of atoms/ Bav (Å^2)	6647/ 103.43	3348/ 69.36	3451/ 52.81
Protein	6575/ 103.15	3285/ 69.65	3342/ 53.178
Ligand	63/ 153.38	36/ 64.72	63/ 44.77
Zinc	4/ 79.47	1/ 46.91	1/ 49.87
Mg	2/ 102.48	-	2/ 38.56
Water molecules	3/ 51.26	26/ 39.60	39/ 35.34
Ramachandran plot (%)			
Favoured /outliers	88.8/ 0.0	92.8/ 0.3	91.7/ 0.3
r.m.s. deviations			
Bonds/Angles (Å/º)	0.007/1.18	0.008/1.29	0.006/1.22
PDB accession codes	5MWL	5MWM	5MW8
Missing residues in pdb	A: 1-4/99-102/221-225/296-311/413-426/465-468 B: 1-7/36-43/97-105/221-226/244-251/277-278/298-311/412-426/464-468	1-9/40-41/122-128/221-228/244-248/298-310/411-419/465-468	1-4/41-42/122-128/221-228/244-245/296-310/411-419/465-468

† $R_{merge} = \Sigma_{hkl} \Sigma_i | I_i(hkl) - [I(hkl)]| / \Sigma_{hkl} \Sigma_i I_i(hkl)$, where $I_i(hkl)$ is the measurement of reflection hkl and [I(hkl)] is the weighted mean of all measurements.

†† $R_{pim} = \Sigma_{hkl} [1/(N - 1)] 1/2 \Sigma_i | I_i(hkl) - [I(hkl)]| / \Sigma_{hkl} \Sigma_i I_i(hkl)$, where N is the redundancy for the hkl reflection.

††† $R_{work} / R_{free} = \Sigma_{hkl} | Fo - Fc | / \Sigma_{hkl} | Fo |$, where Fc is the calculated and Fo is the observed structure factor amplitude of reflection hkl for the

working / free (5%) set, respectively.

FIGURE LEGENDS

FIGURE 1. Structure of *m*IP$_5$ 2-K. *A,* cartoon representation of the structure of *m*IP$_5$ 2-K. The N-lobe and C-lobe are shown in orange-brown and blue colors respectively. ATP and IP$_5$ are shown as green sticks, highlighting the O, N and P atoms in red, blue and orange respectively. The Zn and Mg ions as red and green spheres respectively. The left inset shows a second Zinc Site found in one of the complexes. The dashed lines show disordered regions. In the right, the five helical segments found in *m*IP$_5$ 2-K are detailed. *B,* Arrows indicate β-strands and rectangles the alpha helices. The connecting loops between C-lobe β-sheet and CIP-lobe are highlighted in grey. Conserved sequence motifs within the IPK family are concentrated in the CLs-β-strands connections (CL1: ^{136}EIKPK; CL2: ^{206}QNNXRXF; CL3:variable in sequence and length; CL4: ^{400}DCSIMI and CL5: ^{436}LDLDLK).

FIGURE 2. Substrate recognition by *m*IP$_5$ 2-K. *A,* a zoom of Fig. 1*A* showing the substrates ATP and IP$_5$ and the residues involved in their recognition as sticks in light orange (N-lobe), blue (C-lobe) and grey (CLs in C-lobe). *B,* a zoom showing the nucleotide site. Water molecules are shown as red spheres. *C,* a zoom showing the inositide site. *D,* a zoom showing inositide and nucleotide interaction.

FIGURE 3. Enzyme assays and reaction catalyzed by *m*IP$_5$ 2-K samples. *A,* Kinetic parameters of LSLt-mIP$_5$ 2-K WT and of K173A variant. *B,* kinase reaction catalyzed by *m*IP$_5$ 2-K. Products of enzyme assays resolved by ion exchange HPLC: substrate, Ins(1,3,4,5,6)P$_5$ (IP$_5$) (upper panel); and reaction products after 60 min (middle panel) and 260 min (lower panel) of incubation of IP$_5$ and ATP with enzyme. *C,* reversibility of reaction catalyzed by *m*IP$_5$ 2-K. Products of enzyme assays resolved by ion exchange HPLC: substrate, IP$_6$ (upper panel), reaction products after 110 min (upper middle panel) and 310 min (lower middle panel) of incubation of IP$_6$ and ADP with enzyme. The lower panel shows inositol phosphate (IP) standards obtained by acid hydrolysis of IP$_6$.

FIGURE 4. Zinc binding sites located in *m*IP$_5$ 2-K complexes. *A,* a cartoon representation of *m*IP$_5$ 2-K Zn1 site and *B,* of Zn2 site. *C,* plot of IP$_5$ dependent conversion from ATP to ADP of *m*IP$_5$ 2-K WT and mutants of the zinc binding residues. Error bars show the standard deviation. *D,* zinc content of mutated *m*IP$_5$ 2-K samples relative to WT *m*IP$_5$ 2-K. *E,* Far-UV CD spectra (left) and thermal denaturation followed by CD (right) of WT (black squares) and C291S (blue circles) ΔC-*m*IP$_5$ 2-K.

FIGURE 5. Structural alignment of *m*IP$_5$ 2-K *vs* *At*IP$_5$ 2-K. The secondary structure is shown on top (mammal enzyme) and bottom (plant enzyme). Identical regions are red-shaded, while similar regions are shown in red letters. Light-green shaded squares show regions with a divergent structure in both enzymes. Helical regions inserted into the β-sheet cores are marked as dashed lined boxes.

FIGURE 6. Novel regions of *m*IP$_5$ 2-K and structural comparison with *At*IP$_5$ 2-K. *A,* a cartoon representation of *m*IP$_5$ 2-K (white) and *At*IP$_5$ 2-K (wheat) superposed structures. Zinc ions are shown as dark blue (*m*IP$_5$ 2-K) and cyan (*At*IP$_5$ 2-K) spheres. Mg ions are shown as spheres in similar color to the isoform they belong. The main differences between both samples (D1, D2 and D3) are highlighted in different colors. *B,* representation of N-lobes from both isoforms highlighting D1 (green) insertion in *At*IP$_5$ 2-K. *C,* a piece of CIPII lobe showing D2 in *m*IP$_5$ 2-K (blue). *D,* A view showing D3 (magenta in *m*IP$_5$ 2-K and cyan in *At*IP$_5$ 2-K). *E,* intramolecular interactions produced by D2 in *m*IP$_5$ 2-K. Blue, pink and yellow sticks show residues from D2, D3 and the rest of the protein respectively. *F,* intramolecular interactions produced by D3 in *m*IP$_5$ 2-K. *G,* intramolecular interactions produced by D1 in *At*IP$_5$ 2-K. Green sticks show residues from D1. *H,* plot of IP$_5$ dependent conversion of ATP to ADP of WT *m*IP$_5$ 2-K and several mutants of residues located in the different regions. Error bars show the standard deviation.

FIGURE 7. Analysis of relevant residues for *m*IP$_5$ 2-K function. *A,* plot of IP$_5$ dependent conversion of ATP to ADP by *m*IP$_5$ 2-K WT and several mutants to determine the effect of selected inositide binding residues. Error bars show the standard deviation. *B,* same as A to check the effect of catalytic residues. The squared picture illustrates the salt-bridge between Asp439 and Arg33. *C,* IP$_5$ 2-K sequence conservation across the kingdoms in regions comprising the mutated residues (Asn18 and Lys19; Arg173 and Asp439). Letter X and asterisks denote residues non-conserved or mostly full conserved respectively. Abbreviations: MAM: mammals, VER: vertebrates other than mammals, INV: invertebrates, FUN: Fungi, PLA: Plants.

FIGURE 8. Basic patch on *m*IP$_5$ 2-K surface. *A,* electrostatic surface representation of *m*IP$_5$ 2-K showing its exposed basic patch. Residues conserved and non conserved with the *At*IP$_5$ 2-K are shown in yellow and white respectively. *B,* same representation as in A for the *At*IP$_5$ 2-K enzyme.

Figure 1

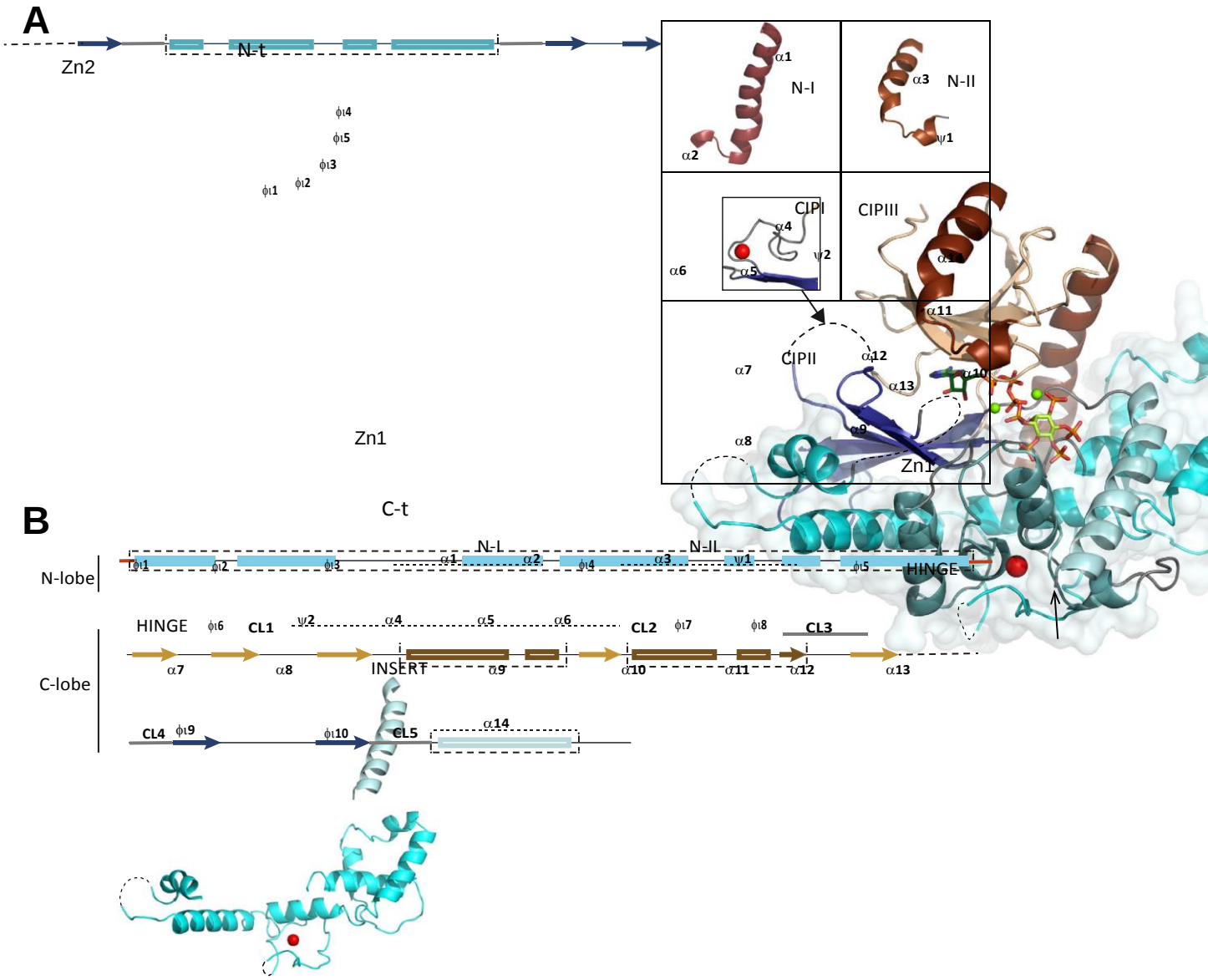
A
Zn2
N-t
N-I
N-II
CIPI
CIPII
CIPIII
Zn1
B
C-t
N-lobe
C-lobe
HINGE
CL1
CL2
CL3
CL4
CL5
INSERT

Figure 2

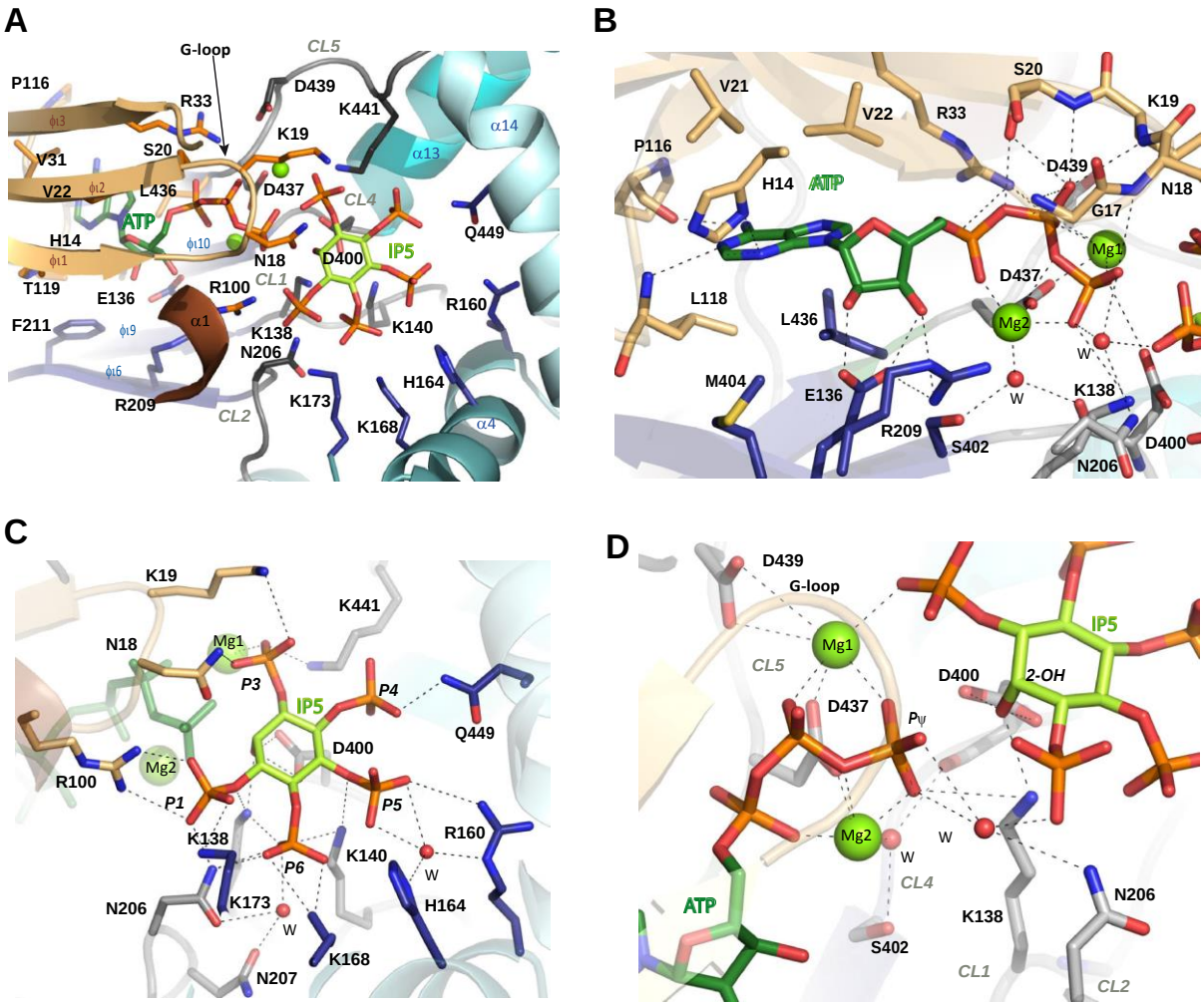
A
G-loop
CL5
P116
R33
D439
K441
K19
S20
V31
V22
L436
D437
CL4
ATP
H14
Q449
N18
D400
IP5
T119
E136
R100
CL1
R160
F211
K138
K140
N206
H164
R209
CL2
K173
K168
α14
α13
α1
α4
B
V21
S20
K19
V22
R33
P116
H14
ATP
D439
N18
G17
Mg1
D437
L118
L436
Mg2
M404
E136
K138
R209
S402
D400
N206
C
K19
K441
N18
Mg1
P3
P4
IP5
Q449
D400
Mg2
R100
P1
P5
K138
R160
P6
K140
N206
K173
H164
K168
N207
D
D439
G-loop
IP5
Mg1
CL5
D400
2-OH
D437
Pψ
Mg2
CL4
ATP
K138
N206
S402
CL1
CL2

Figure 3

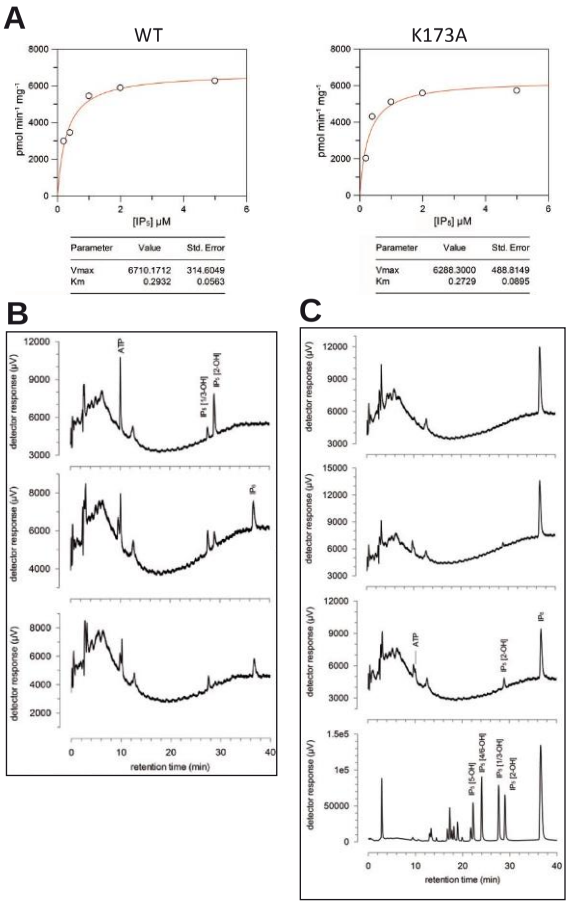
A
WT
K173A
pmol min-1 mg-1
[IP5] µM
Parameter Value Std. Error
Vmax 6710.1712 314.6049
Km 0.2932 0.0563
Parameter Value Std. Error
Vmax 6288.3000 488.8149
Km 0.2729 0.0895
B
C
detector response (µV)
retention time (min)
ATP
IP5 [1/3-OH]
IP5 [2-OH]
IP5
IP5 [5-OH]
IP5 [4/6-OH]

Figure 4

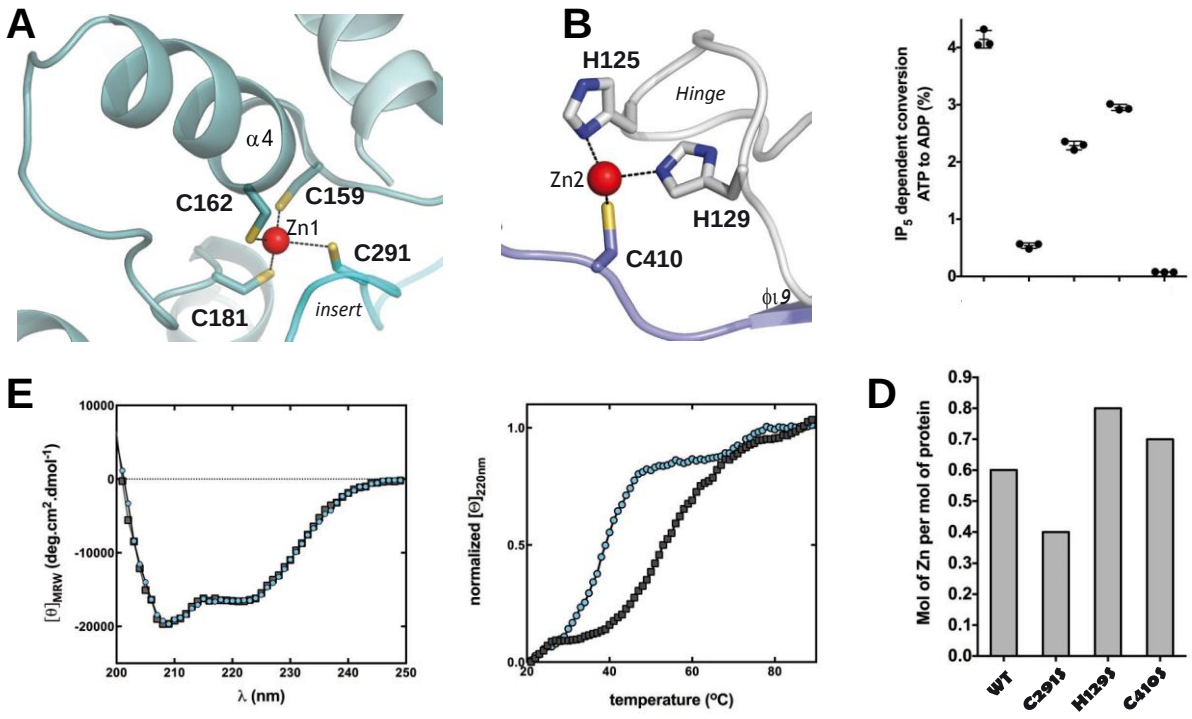
A
α4
C162
C159
Zn1
C291
C181
insert
B
H125
Hinge
Zn2
H129
C410
ϕι9
IP5 dependent conversion ATP to ADP (%)
E
[θ]MRW (deg.cm2.dmol-1)
λ (nm)
normalized [Θ]220nm
temperature (°C)
D
Mol of Zn per mol of protein
WT
C291$
H129$
C410$

Figure 5

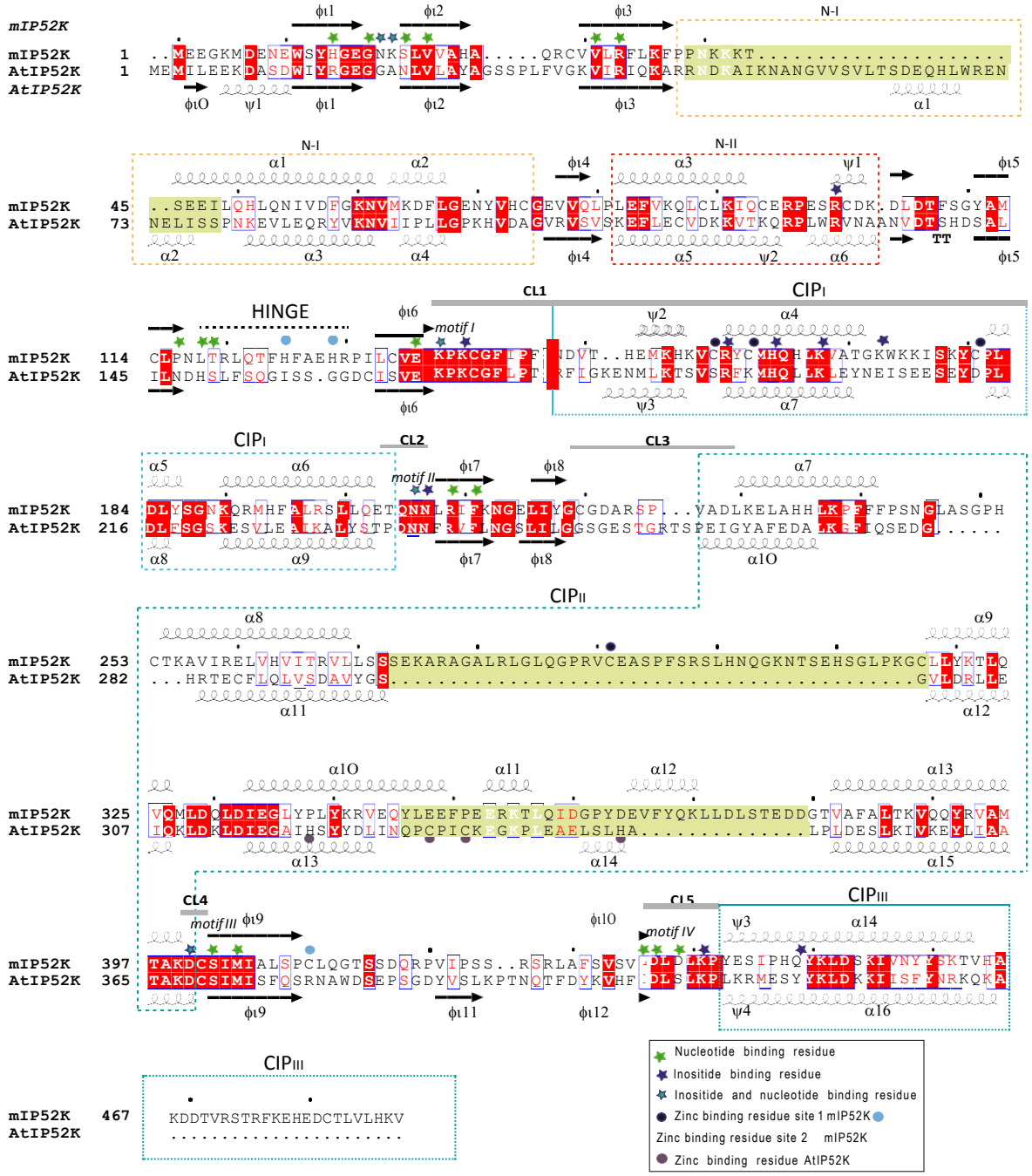
mIP52K
AtIP52K
N-I
N-II
HINGE
CL1
CL2
CL3
CL4
CL5
CIPI
CIPII
CIPIII
motif I
motif II
motif III
motif IV
Nucleotide binding residue
Inositide binding residue
Inositide and nucleotide binding residue
Zinc binding residue site 1 mIP52K
Zinc binding residue site 2 mIP52K
Zinc binding residue AtIP52K

Figure 6

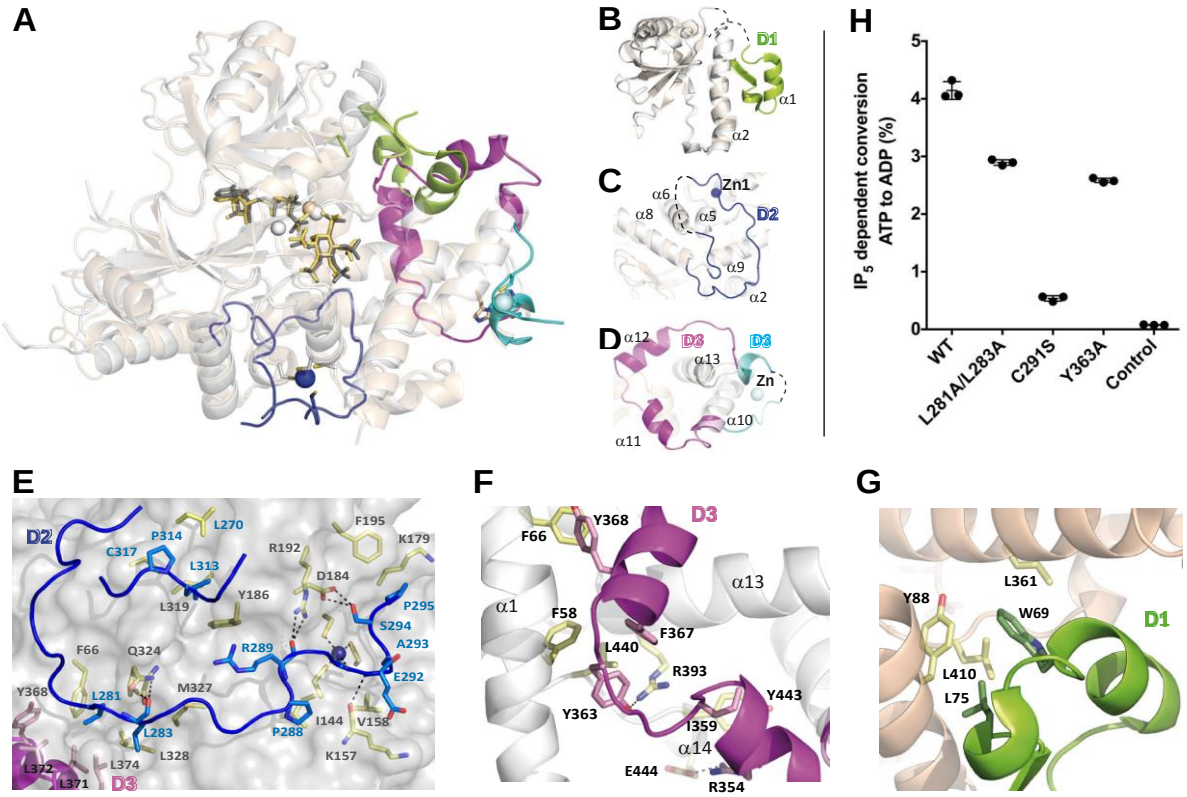
A
B
D1
α1
α2
C
α6
Zn1
α8
α5
D2
α9
α2
D
α12
D3
D3
α13
Zn
α10
α11
H
IP5 dependent conversion ATP to ADP (%)
5
4
3
2
1
0
WT
L281A/L283A
C291S
Y363A
Control
E
D2
P314
L270
F195
K179
C317
R192
L313
D184
Y186
L319
P295
S294
A293
F66
Q324
R289
E292
Y368
L281
M327
I144
V158
L283
P288
L328
K157
L372
L374
L371
D3
F
D3
Y368
F66
α13
α1
F58
F367
L440
R393
Y443
Y363
I359
α14
E444
R354
G
L361
Y88
W69
D1
L410
L75

Figure 7

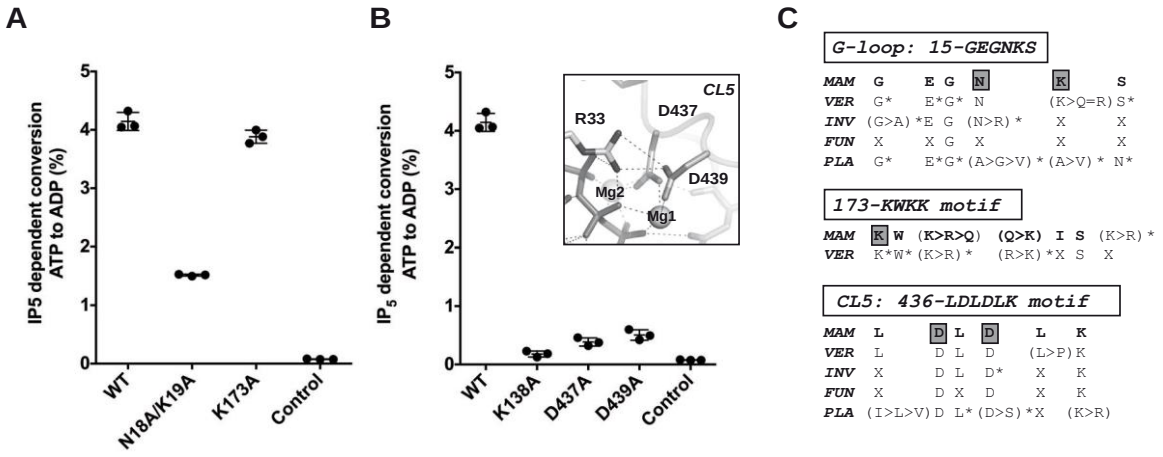
A
IP5 dependent conversion ATP to ADP (%)
WT
N18A/K19A
K173A
Control
B
IP5 dependent conversion ATP to ADP (%)
WT
K138A
D437A
D439A
Control
CL5
R33
D437
D439
Mg2
Mg1
C
G-loop: 15-GEGNKS
MAM G E G N K S
VER G* E*G* N (K>Q=R)S*
INV (G>A)*E G (N>R)* X X
FUN X X G X X X
PLA G* E*G*(A>G>V)*(A>V)* N*
173-KWKK motif
MAM K W (K>R>Q) (Q>K) I S (K>R)*
VER K*W*(K>R)* (R>K)*X S X
CL5: 436-LDLDLK motif
MAM L D L D L K
VER L D L D (L>P)K
INV X D L D* X K
FUN X D X D X K
PLA (I>L>V)D L*(D>S)*X (K>R)

Figure 8

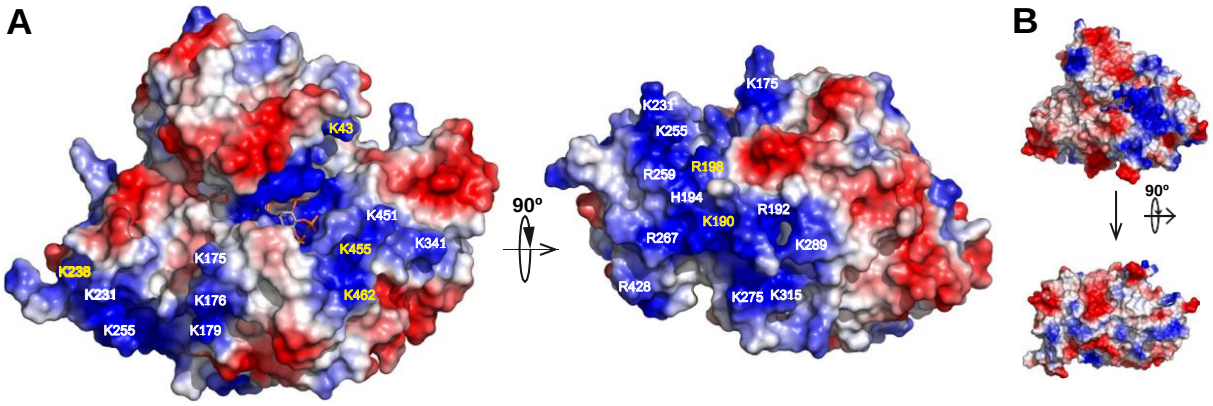
A
K43
K451
K455
K341
K175
K238
K231
K176
K462
K255
K179
90°
K175
K231
K255
R259
R198
H194
K190
R192
R267
K289
R428
K275
K315
B
90°